

# Fusing Multiple Neuroimaging Modalities to Assess Group Differences in Perception–Action Coupling

By JORDAN MURASKIN, JASON SHERWIN, GREGORY LIEBERMAN, JAVIER O. GARCIA, TIMOTHY VERSTYNEN, JEAN M. VETTEL, AND PAUL SAJDA, *Fellow IEEE*

**ABSTRACT** | In the last few decades, noninvasive neuroimaging has revealed macroscale brain dynamics that underlie perception, cognition, and action. Advances in noninvasive neuroimaging target two capabilities: 1) increased spatial and temporal resolution of measured neural activity; and 2) innovative methodologies to extract brain–behavior relationships from evolving neuroimaging technology. We target the second. Our novel methodology integrated three neuroimaging methodologies and elucidated expertise-dependent differences in functional (fused EEG–fMRI) and structural (dMRI) brain networks for a perception–action coupling task. A set of baseball players and controls performed a Go/No-Go task

designed to mimic the situation of hitting a baseball. In the functional analysis, our novel fusion methodology identifies 50-ms windows with predictive EEG neural correlates of expertise and fuses these temporal windows with fMRI activity in a whole-brain 2-mm voxel analysis, revealing time-localized correlations of expertise at a spatial scale of millimeters. The spatiotemporal cascade of brain activity reflecting expertise differences begins as early as 200 ms after the pitch starts and lasts up to 700 ms afterwards. Network differences are spatially localized to include motor and visual processing areas, providing evidence for differences in perception–action coupling between the groups. Furthermore, an analysis of structural connectivity reveals that the players have significantly more connections between cerebellar and left frontal/motor regions, and many of the functional activation differences between the groups are located within structurally defined network modules that differentiate expertise. In short, our novel method illustrates how multimodal neuroimaging can provide specific macroscale insights into the functional and structural correlates of expertise development.

**KEYWORDS** | Diffusion tensor imaging; encephalography; machine learning; magnetic resonance imaging; sensor fusion

Manuscript received February 8, 2016; revised April 28, 2016; accepted May 22, 2016. This work was supported by the National Institutes of Health under Grants R01-MH085092 and T35-AG044303, and the U.S. Army Research Laboratory under Cooperative Agreement W911NF-10-2-0022.

**J. Muraskin, J. Sherwin,** and **P. Sajda** are with the Department of Biomedical Engineering, Columbia University, New York, NY 10027 USA (e-mail: psajda@columbia.edu).

**G. Lieberman** is with the Human Research and Engineering Directorate, U.S. Army Research Laboratory, Aberdeen Proving Ground, MD 20783 USA, and also with the Department of Bioengineering, University of Pennsylvania, Philadelphia, PA 19104 USA.

**J. O. Garcia** is with the Human Research and Engineering Directorate, U.S. Army Research Laboratory, Aberdeen Proving Ground, MD 20783 USA.

**T. Verstynen** is with the Department of Psychology, Carnegie Mellon University, Pittsburgh, PA 15213 USA.

**J. M. Vettel** is with the Human Research and Engineering Directorate, U.S. Army Research Laboratory, Aberdeen Proving Ground, MD 20783 USA, with the Department of Bioengineering, University of Pennsylvania, Philadelphia, PA 19104 USA, and also with the Department of Psychological & Brain Sciences, University of California, Santa Barbara, Santa Barbara, CA 93106 USA.

Digital Object Identifier: 10.1109/JPROC.2016.2574702

This work is licensed under a Creative Commons Attribution 3.0 License. For more information, see <http://creativecommons.org/licenses/by/3.0/>

## I. INTRODUCTION

Noninvasive neuroimaging of structure and function has been used for decades to better characterize and understand how our perceptions relate to our actions.

Although new technologies are being developed to image the living brain, from optical methods to new types of nanoprobe and sensors [1]–[3], observing *in vivo* activity in the healthy human brain will be mostly based on magnetic resonance (MRI) and electromagnetic imaging methods for the foreseeable future. In terms of functional imaging, both electroencephalography (EEG) and blood-oxygen-level-dependent functional magnetic resonance imaging (BOLD fMRI) are extremely common noninvasive methods for observing human brain function. Magnetoencephalography (MEG), a close cousin of EEG, is also used to noninvasively measure brain activity, though its costs are more prohibitive than EEG. EEG and fMRI also can be acquired simultaneously, which is appealing given that both methods are complementary in terms of their basic physiological measurements. EEG is a direct measurement of neural “mass” activity and provides high temporal resolution and dynamics (at time-scales of milliseconds) while fMRI is an indirect measurement of neural activity, based on hemodynamic changes, and offers high spatial resolution given its noninvasive acquisition (spatial resolution in millimeters). Separately, these modalities have made enormous contributions to human behavioral, psychological, and clinical neuroscience. When leveraged in a fused representation, for example when simultaneously acquired, they have been shown to provide new insight into the macroscale dynamical networks that underlie function in the human brain [4]–[11].

In addition to function, understanding the structural organization of the human brain is central to understanding why some brains may function differently than others. Classically, structural differences underlying experience-dependent plasticity were thought to occur in the gray matter regions of the cortex, but recently, research has suggested that neural adaptations can be seen in the white matter fiber tracts as well [12], [13]. A diffusion MRI (dMRI) scan captures the directional diffusion of water within a voxel, and the location and direction of the white matter tracts are inferred from the constrained movement of water molecules (see [14] for a review). Changes in fiber tract connections have been found over a range of temporal scales, including research on professional concert pianists in their thirties that found that differences in fiber tract organization reflected the number of practicing hours during adolescence [15], while another study found structural effects in adults after six weeks of juggling practice [16]. Converging evidence from across the lifespan indicates that variability in white matter fiber tract connections correlates with between subject variability in task performance [17], [18].

In this paper, we demonstrate, with a comprehensive example, that an integrated analysis of fused EEG-fMRI functional imaging together with structural DTI provides unique insight into difference in brain networks between groups of individuals having different perception-action

coupling proficiencies. Our specific example focuses on differences in perception-action coupling between experts (i.e., baseball players) and a nonexpert control group during a Go/No-Go task based on baseball pitch discrimination. Deciding on whether to swing at an incoming baseball pitch is a complex task with a very low success rate worth millions of dollars. To be able to quickly predict a 90-mph pitch trajectory and have the motor control to place a bat on the 3-in diameter ball in less than 400 ms has been referred to as “clearly an impossible task” [19]. However, after hours of training, many professional athletes are able to succeed (although with at best a 1/3 success rate) and have become experts in this specific type of perception-action coupling.

Recently our group has shown, using only EEG, that temporally specific neural correlates of a rapid Go/No-Go decision differed between players versus controls [20]. Players, overall, performed better at the task compared to controls both in terms of accuracy and faster response times, i.e., players shifted their speed-accuracy tradeoff curve instead of moving along the same curve as defined by the controls. Players also showed differences in their task-evoked EEG components. Players had larger and earlier EEG components for Correct Go and Correct No-Go trial types, relative to controls. These differences were found to be most likely in the inhibition response during the No-Go trials. Source localization suggested that players have stronger cortical sources in the supplementary motor area (SMA) for Correct No-Go trials and the fusiform gyrus for Correct Go trials. This work offered evidence that there are distinct spatiotemporal neural differences between baseball players and controls during a baseball-like perceptual decision making task. However, the EEG, by itself, only provides a partial picture and does not enable a comprehensive investigation of the structural and functional networks underlying these differences.

Below we describe an approach and corresponding results that use whole brain BOLD fMRI and simultaneously collected EEG and confirms these previous player versus control differences found in our EEG-only experiments [20]. In addition, we describe novel EEG/fMRI fusion techniques and apply these to this data set as a way to further elucidate functional networks underlying differences in this particular type of expertise. Specifically, a single-trial sliding window linear discrimination analysis of the EEG is used to construct a temporally precise, neurally-derived rating of expertise for each subject. The rating is used as a covariate of interest in the fMRI model, identifying both the regions in the brain that correlate with differences in expertise as well as the timing of these differences. We analyze these results with respect to additional differences we identify in a structural network analysis, enabled by advanced connectivity methods informed by the functional analysis. We conclude that advances in understanding the human

brain will be enabled by a more integrated analysis of structural and functional neuroimaging within the context of complex behavior.

## II. NEUROIMAGING DATA COLLECTION AND METHODS OF ANALYSIS

### A. Subjects

The study included 14 division I collegiate baseball players (all male,  $19.57 \pm 2.4$  years) and 24 nonbaseball player controls (all male,  $20.92 \pm 2.7$  years) with an age range of 18–30 years. Three of the controls were not used in the task-based analysis due to movement during the fMRI scanning and one expert was excluded from structural analysis due to low quality diffusion image reconstruction. Controls had no professional or collegiate baseball experience. All subjects reported no history of neurological problems and had normal or corrected vision and all gave informed consent according to the guidelines and approval of the Columbia University Institutional Review Board.

### B. Behavioral Paradigm

This behavioral paradigm has been applied and described previously in [20] and [21] and is reproduced here for completeness.

The experimental session involves a training session prior to the simultaneous fMRI/EEG data acquisition. In the training, subjects familiarized themselves with the different pitch types and completed practice trials until they scored an accuracy of at least 60% (above the random chance accuracy of 50%). At the beginning of each trial, a single letter corresponding to the pitch (“F” for fastball, “C” for curveball, and “S” for slider) was shown on the screen (Horizontal view  $0.28^\circ$  and vertical view  $0.28^\circ$ ) for a mean time of  $819 \pm 3.1$  ms. While the letter was on the screen, a horizontal bar (horizontal extent  $3.93^\circ$ , vertical  $0.28^\circ$ ) shrank (horizontally) at a constant rate to either the left or right side of the screen. If the pitch following the letter cue came from a left handed pitcher, then the horizontal bar shrank toward the right, and if the pitch came from a right handed pitcher, then the horizontal bar shrank toward the left. After the horizontal bar shrank completely to either the left or the right, the pitch started from that point on the left or right side of the screen (i.e., pitches from left-handed pitchers started from the right side of the screen, and *vice versa*).

Subjects used the VisuaStim Digital System (Resonance Technology)  $600 \times 800$  goggle display to view 450 simulated baseball pitches (five blocks of 90 trials, three different types of pitches) from the viewpoint of a baseball catcher (at the end of the baseball’s trajectory). While viewing these pitches, subjects completed a Go/No-Go task by determining if each pitch matched its

prestimulus cue. The program optseq2 [22] was used to select a mean jittered interstimulus interval (ISI) that enabled the rapid presentation of fMRI events without overlap from the hemodynamic responses (mean of 3000 ms and SE of 225 ms). Each subject was instructed to respond by pressing a keyboard button with the index finger of his right hand if the prestimulus cue matched the type of pitch that followed it (“Go” trials). In addition, in order for a “Go” response to be correct, the subject needed to respond while the ball was still in the screen. If the prestimulus cue and the pitch did not match, the subject was instructed to withhold his response (“No-Go” trials). Feedback was given after every trial (for both “Go” and “No-Go” trials) in the form of a “+” for correct responses in “Go” trials and correct withholding of responses in “No-Go” trials and a “-” for incorrect “Go” and “No-Go” responses. 60% of the trials were “Go” and 40% of the trials were “No-Go.”

Overall accuracy for the task was determined by calculating the percent of trials with a correct response (the subject responded while the ball was still on the screen for “Go” trials and withheld his response for “No-Go” trials). Go accuracy was determined by calculating what percent of all the “Go” trials had a correct response (subject responded and this response happened while the ball was still on the screen). “No-Go” accuracy was determined by calculating what percent of all the “No-Go” trials the subject correctly withheld his response.

Similar to our previous work, we simulated each pitch via a differential equation solver in Matlab 2010a (Mathworks, Natick, MA, USA) (see [20]–[23] for details) and presented these using PsychToolbox [24]. Pitches were simulated using six-coupled differential equations. Each of the three pitches—fastball, curveball, and slider—have well-defined initial conditions. To create each pitch, we varied the initial velocity and the rotation angle. For each simulated pitch, an isoluminant green circle was plotted on a gray background for every frame of the trajectory. The size of the circle increased as it approached the viewer, so as to give the illusion of depth. When the ball crossed “home plate,” the circle disappeared.

### C. Structural MRI and Simultaneous fMRI-EEG

#### Data Acquisition

A 3T Philips Achieva MRI scanner (Philips Medical Systems) with an eight-channel SENSE head coil was used to collect MRI data. For each task block, functional echo planar imaging (EPI) data sensitive to blood oxygenated level-dependent (BOLD) contrast were collected (2-s TR, 20-ms TE,  $64 \times 64$  matrix, and 35 interleaved slices, 240 repetitions). After the task based data collection, a 5-min resting state scan was collected. Whole brain T1-weighted anatomical images ( $1 \times 1 \times 1$  mm) and single high volume EPI images ( $2 \times 2 \times 2$  mm) were also obtained to help with registration. DTI was acquired

along 50 directions with a b-value of  $1500 \text{ s/mm}^2$  (as well as one image with no diffusion weighting) with a voxel-size of  $2 \times 2 \times 2 \text{ mm}^3$  (TR = 8996 ms, TE = 80 ms, FOV = 224 mm, 75 axial slices AC/PC aligned encompassing the whole brain, SENSE Factor = 2).

Simultaneous and continuous EEG data were acquired with a custom built MR-compatible EEG system [7], [9], [25]. This system included a differential amplifier and a bipolar EEG cap with 36 Ag/AgCl electrodes (including the left and right mastoids) arranged as 43 bipolar pairs. In order to minimize noise from subject head motion in the main magnetic field and from inductive pickup from magnetic gradient pulses, we used twisted bipolar pair leads. The 488-Hz-sampled EEG was synchronized with the scanner clock at the start of each functional image acquisition by sending a transistor-transistor logic (TTL) pulse to the recording computer. This was used in the gradient artifact removal during the offline EEG data preprocessing steps. 10-k $\Omega$  resistors were built into each electrode to ensure subject safety, and all electrode impedances were kept below 20 k $\Omega$ .

#### D. EEG Preprocessing

EEG preprocessing was done with Matlab (Mathworks, Natick, MA, USA). First, gradient artifact removal was performed using a template subtraction algorithm [7]. Then, a software-based 0.5-Hz high-pass filter was used to remove direct current (dc) drifts, a 60-Hz (harmonic) notch filter to minimize line noise artifacts, and a 100-Hz low-pass filter were applied before resampling the data to 256 Hz. These filters were designed to be zero phase to minimize delay distortions. Stimulus events—i.e., countdown, pitch type, responses—were recorded on separate channels.

After filtering, ICA was run using EEGLAB [26] and the FastICA [27] algorithm to remove eye-blink artifacts and other non-EEG artifacts. In stimulus-locked epoching (from 1500 to 2000 ms), the average baseline was removed using data from 200 to 0 ms. An automatic artifact epoch rejection algorithm from EEGLAB was run to remove all epochs that exceeded a probability threshold of five standard deviations from the average. Trials where the subject's response time (RT) was earlier than 100 ms from pitch onset were excluded from further analysis.

Ballistocardiogram (BCG) artifacts were removed from the continuous gradient-free data using a principal components analysis method [7], [25]. First, the data were low passed at 4 Hz to extract the signal within the frequency range in which BCG artifacts are observed and then the first two principal components were determined. The channel weightings corresponding to those components were projected onto the broadband data and subtracted out. These BCG-free data were then rereferenced from the 43 bipolar channels to the 34-electrode space to calculate scalp topographies of EEG discriminating components.

#### E. Behavioral Analysis

Percent error rates and RTs were analyzed. Errors were broken down into both omissions and commissions, i.e., no-responses and late responses in Go trials and button presses in No-Go trials. Repeated-measures ANOVAs on each behavioral measure were carried out using Trial type (two levels: Go, No-Go) as the within-subject factor and group (player/control) as the between subject factor. The Greenhouse-Geisser (GG) epsilon correction was applied to adjust the degrees of freedom of the F ratios where necessary, and *post hoc* comparisons were also made in order to determine the significance of contrasts by applying the Bonferroni procedure ( $\alpha = 0.05$ ).

#### F. Single-Trial Analysis of EEG

Our analysis focused on a single-trial approach to discriminate between a set of stimulus or response conditions. First, we considered only behaviorally correct trials. Regularized logistic regression was used as a linear classifier to find an optimal projection for discriminating between behaviorally correct Go and behaviorally correct No-Go trials over a specific temporal window [28]. This approach has been previously applied to identify neural components underlying rapid perceptual decision making [7], [9], [20], [23], [29]. Specifically, we defined a training window starting at either a prestimulus or poststimulus onset time  $\tau$ , with a duration of  $\delta$ , and used logistic regression to estimate a spatial weighting vector that maximally discriminates between EEG sensor array signals  $X$  for each class (e.g., Go versus No-Go trials)

$$y_\tau = w_\tau^T X_{\tau\delta}. \quad (1)$$

In (1),  $X$  is an  $N \times T$  matrix ( $N$  sensors and  $T$  time samples). The result is a “discriminating component” that is specific to activity correlated with each condition, while minimizing activity correlated with both task conditions. For our experiments, the duration of the training window ( $\delta$ ) was 50 ms and the center of the window ( $\tau$ ) was varied across time in 25-ms steps. We used the re-weighted least squares algorithm to learn the optimal discriminating spatial weighting vector [30]. We quantified the performance of the linear discriminator by the area under the receiver operator characteristic (ROC) curve, referred to here as AUC, using a leave-one-out procedure. We used the ROC AUC metric to characterize the discrimination performance as a function of sliding our training window from 0-ms prestimulus to 1000-ms poststimulus (i.e., varying  $\tau$ ).

We quantified the statistical significance of AUC in each window ( $\tau$ ) using a label permutation procedure. We randomized the labels for each trial (i.e., trial was a Correct Go or a Correct No-Go) and retrained the classifier. This was done 1000 times for each subject, and the

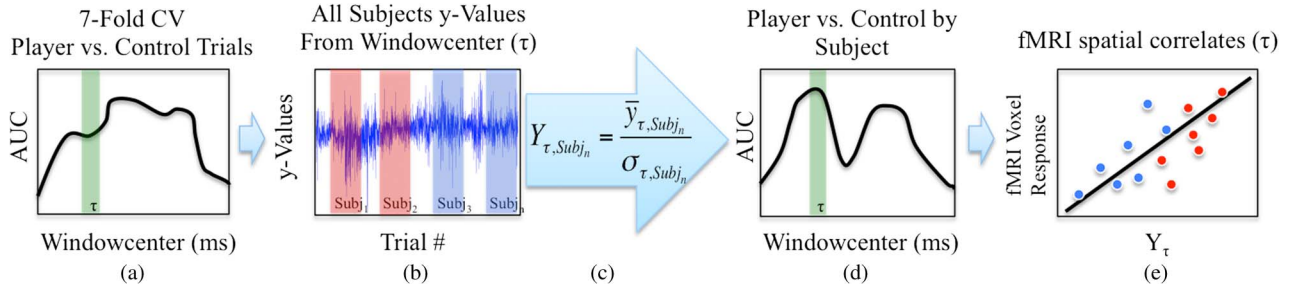


**Fig. 1. Illustration of player/control EEG-fMRI data fusion methodology.** (a) First, a sevenfold sliding window logistic regression classifying EEG player trials from control trials across all subjects. These can be either Correct Go or Correct No-Go trials. The sliding window logistic regression produces an area under the receiving operator curve (AUC) for each window analyzed. For each window center  $\tau$ , the distance to the discriminating hyperplane ( $y$ ) for each trial is calculated (b). (c) Each subject's  $y$ -values are averaged and divided by their standard deviation producing a matrix  $Y_{\tau,Subj_n}$ . (d) These  $Y$ -values are then used to construct sliding window AUC metrics by comparing how well the  $Y$ -values predict subject expertise. (e) Significant window center  $Y$ -values are then used as regressors in the fMRI general linear model to find the spatial components of expertise at that time window.

AUC values from these permutations were used to establish a p-value for the mean AUC in each time window. All significant results have been corrected for multiple comparisons using a Bonferroni correction at  $p < 0.05$ .

### G. fMRI Preprocessing

Using FSL (FMRIB Software Library; [31]), we performed bias-field correction on all images to adjust for field distortion artifacts caused by the EEG wires. We then performed slice-timing correction, motion correction, 0.01-Hz high-pass filtering, and 5-mm full-width half-maximum spatial smoothing on the functional data. Motion correction provided motion parameters that were included as confounds in the subsequent GLM. To help reduce noise in our fMRI data, MELODIC de-noising was applied to the functional data using the methodology described in [32]. Functional and structural images were then registered to a standard Montreal Neurological Institute (MNI) brain template after brain extraction, and each subject's image registration was checked manually to ensure proper alignment.

### H. Player Versus Control Traditional fMRI Analysis

We first ran a traditional fMRI analysis using event-related and RT variability regressors in a GLM. The event-related regressors were composed of boxcar functions with unit amplitude and onset and offset matching those of the stimuli (Correct Go, Correct No-Go, Incorrect No-Go, and a bad trial/Incorrect Go trial regressors). RT variability was modeled using parametric amplitude boxcars with onset/offset matching the stimulus, and these were orthogonalized to the respective event-related regressors. Orthogonalization was performed in FSL using its Gram-Schmidt procedure [33] to decorrelate the RT regressor from all other event-related regressors. All regressors were convolved with the canonical hemodynamic response function (HRF), and temporal derivatives were included as confounds of no interest. A fixed effects

model was used to model activations across runs, and a mixed effects approach (FLAME 1 + 2 [31]) was used to compute the contrasts for traditional players versus controls to identify activation patterns for the Correct Go and Correct No-Go conditions as well as the difference between Correct Go versus Correct No-Go contrasts. Statistical image results for these traditional analyses were thresholded at  $z > 1.8$ , and clusters were corrected for multiple comparisons at  $p = 0.05$  [34], [35].

### I. Player Versus Control EEG-fMRI Fusion Analysis

We created a novel methodology to fuse EEG-fMRI data and study group differences. First, we identify time windows in the EEG signal that discriminate between players and controls, and we then use these time windows as regressors in a GLM analysis of the fMRI data.

In accordance with previous methods [7], [9], [10], our methodology uses EEG trial-to-trial variability to index a brain signal of interest and predict subject expertise between players and controls. First, a sliding window linear discrimination analysis, based on logistic regression, was run separately on Correct Go and Correct No-Go trials to classify each trial as belonging to either a player or control. Instead of processing the data within subjects, the time window ( $\tau$ ) data were pooled across subjects to create a data  $n \times s$  matrix,  $n$ -trials (7213 for Correct Go, 2791 for Correct No-Go) by  $s$ -subjects (35). A sevenfold logistic regression was run independently for each trial type, where for each fold the data from one player and two controls were held out for testing. The time window center defining the data input for the logistic regression was varied across the trial, starting from 0 ms from stimulus onset and shifted by 25 ms until the final window at 1000 ms. The accuracies of the classifiers were assessed using the AUC [Fig. 1(a)].

After applying logistic regression to the time windows, each subject's  $y$ -values [see (1) and Fig. 1(b)] were averaged and divided by the standard deviation of the

**Table 1** Mean Behavioral Response Times (RTs) and Error Rates for Players and Controls. Standard Deviations Are in Parentheses

	Go Trials		No-Go Trials	
	RT (ms)	Error Rate (%)	RT(ms)	Error Rate (%)
Players	451.6 (24)	9.93 (3.5)	451.3 (27)	45.24 (9.1)
Controls	477.4 (24)	21.07 (13.9)	479.9 (22.3)	56.77 (13)

individual subject's trial-wise  $y$ -values to create an overall "expertise-rating"  $y$ -value,  $Y_{\tau, \text{Subj}_n}$  [Fig. 1(c)]. For each time window in each data set, the AUC was computed by comparing the overall expertise  $y$ -value,  $Y_{\tau, \text{Subj}_n}$ , to the ground-truth label of player or control. The significance of the AUC for each time window was determined using a permutation test. The label of player or control was randomly assigned 1000 times for each window, the sevenfold logistic regression was performed, and a distribution of values for AUCs with random labels were used to compute a significance threshold for the null hypothesis that there was no EEG marker of expertise. Windows were considered significant if they passed an FDR-corrected threshold of  $p < 0.05$ .

To fuse the EEG results with fMRI, we used time windows that discriminated players from controls in EEG analysis as regressors of interest in a GLM that correlated subject expertise with fMRI activation. Resulting statistical parametric maps for these analyses were thresholded at  $z > 1.8$ , and clusters were corrected for multiple comparison at  $p = 0.05$  [34], [35].

### J. Structural Connectivity Differences Between Player and Control

Diffusion MRI analysis [36] was performed using DSI Studio (<http://dsi-studio.labsolver.org/>) and Matlab (MathWorks, Inc.; Natick, MA, USA) on 37 subjects (13 experts, 24 novices). Diffusion data were reconstructed using  $q$ -space diffeomorphic reconstruction (QSDR [37]) with a diffusion sampling length ratio of 1.25 and an output resolution of 2 mm. Whole-brain fiber tractography [38] was performed 1000 times for each participant to minimize the impact of any bias in the tractography parameter scheme on streamline generation. Across the 1000 iterations, values were randomly sampled for QA-based fiber termination thresholds (between 0.01 and 0.10), turning angle thresholds (between  $40^\circ$  and  $80^\circ$ ), and smoothing (between 50% and 80%) to ensure results are robust to these parameter choices, while using constant values for step size (1 mm) and min/max fiber lengths (10 mm/400 mm). Each iteration generated 250000 streamlines, and with a fixed streamline count, differences in the number of estimated fiber tracts can be

interpreted as differences in the strength of connection [39]. For each subject, we derived a whole brain structural connectivity matrix by averaging the tractography estimates across the 1000 iterations to estimate the strength of connection between all 116 brain regions in the AAL atlas.

The  $116 \times 116$  structural matrix for each subject was used as input in an ROI connectivity analysis. The Louvain modularity algorithm implemented in the Brain Connectivity Toolbox (BCT, [40]) was run on the group average unthresholded streamline connectivity matrix. The order of nodes in the connectivity matrix was reorganized based on the representative modularity partition with five modules. After partitioning, the number of streamline edges differing between groups with a threshold of  $p < 0.05$  uncorrected was assessed for each of the identified modules both for within-module and between-module connections. This type of analysis has been used to identify structural differences between autistic patients and controls [41]. A permutation test was implemented to assess if the distribution of significant edges within and across modules deviated from a null hypothesis that there was no network difference between experts and controls. The label of player or control was randomly assigned 5000 times, and for each permutation, a count of significant edges between and within modules for each group (player > control and control > player) was calculated. Each module-to-module count was then compared to its permutation distribution to determine significance at  $p < 0.05$ .

## III. RESULTS

### A. Behavioral Results

Table 1 presents group data for response times and error rates for Go and No-Go trials. A two-way ANOVA on the response times showed a significant effect for the Group ( $p = 0.0024$ ). Trial type ( $p = 0.24$ ) and the Group  $\times$  Trial interaction ( $p = 0.24$ ) did not pass our significance threshold of  $p < 0.05$ . The two-way ANOVA for error rates showed a significant main effect for Group ( $p < 0.001$ ), Trial Type ( $p < 0.001$ ), but the Group  $\times$  Trial interaction ( $p = 0.944$ ) was not significant.

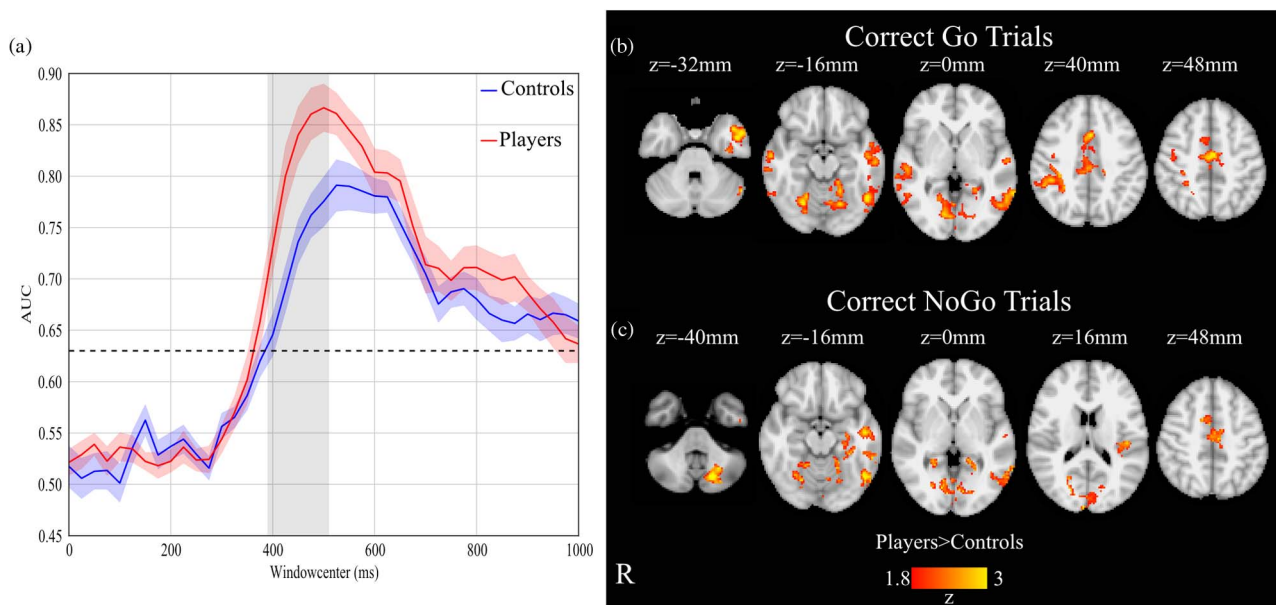


**Fig. 2.** EEG and fMRI traditional results. (a) Sliding window logistic regression results. Stimulus-locked EEG discrimination results for Correct Go versus Correct No-Go trials for controls (blue) and players (red). Each AUC curve shows the mean and standard error bars computed using leave-one-out discrimination. The significance line (dotted) is corrected for multiple comparisons (line at  $p = 0.05$  FDR corrected for 41 time window comparisons). Gray shading indicates which time points showed a significant difference between players and controls [independent groups  $t$ -test at each significant window and an FDR correction for multiple (26) windows]. (b) Group-level results for players having higher activation for the Correct Go trials overlaid on the MNI brain template. (c) Group-level results for players having higher activation for the Correct No-Go trials overlaid on the MNI brain template. Statistical maps were thresholded at  $z > 1.8$ , and clusters were multiple-comparison corrected at  $p = 0.05$ .

## B. Confirming Previous EEG-Only Neural Correlates of Player Versus Control Differences

Given that we acquired our EEG and fMRI simultaneously, which can result in reduced SNR relative to separate acquisitions, we first sought to confirm results we reported in a previous EEG-only acquisition and analysis [20]. Fig. 2(a) shows the mean (across subjects, separated by group) performance (area under the ROC curve: AUC) for stimulus-locked EEG components discriminative of Correct Go versus Correct No-Go discrimination trials. We found that players and controls had similarly shaped discrimination curves; however, players exhibited an earlier rise and larger peak than controls. Both groups showed no significant early discrimination (discrimination before 300 ms); however, discrimination rose sharply to a maximum AUC of 0.87 at 500 ms for players and 0.79 at 525 ms for controls. The players' discrimination curves also were shifted 25 ms earlier relative to that for the controls. To test for significant discrimination differences between players and controls, we computed an independent groups  $t$ -test at each window. Shaded regions indicated significant differences ( $p < 0.05$  FDR corrected) in discrimination activity between players and controls. Players show significantly higher discrimination than controls from 400 to 500 ms. These results are all consistent with our previous EEG-only analysis [20].

## C. Player Versus Control Traditional fMRI Results

We conducted a traditional GLM analysis to demonstrate what an fMRI-only analysis would reveal on the differences between players versus controls. After computing the traditional fMRI contrasts for each subject, an independent two groups  $t$ -test was run comparing the players' and controls' Correct Go and Correct No-Go subject level beta estimates. Significant clusters showing higher activations for players were found in both the Correct Go and Correct No-Go trial types [Fig. 2(b) and (c)]. Activations were located in the temporal fusiform gyrus, middle temporal gyrus, anterior cingulate, presupplementary motor and supplementary motor cortices for Correct Go trials. Similarly for Correct No-Go trials, activations were found in the presupplementary motor area, supplemental motor areas, middle temporal gyrus, and fusiform gyrus.

## D. Unique Functional Network Differences Between Player Versus Control Revealed via EEG-fMRI Fusion

The AUCs for sliding window logistic regression that discriminated expertise in Correct Go and Correct No-Go trials are plotted in Fig. 3(a). Sliding window AUC results for classifying each subject by expertise based on the sevenfold logistic regression  $y$ -values are plotted in Fig. 3

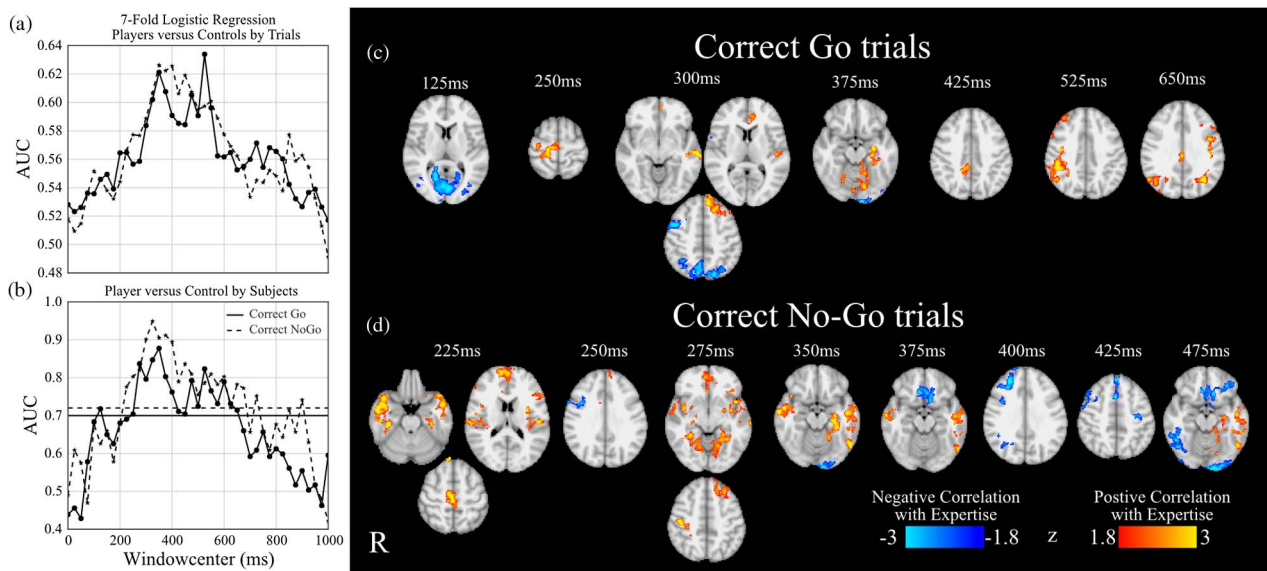


**Fig. 3. Player versus control EEG-fMRI fusion results. (a) Stimulus-locked sevenfold cross-validated EEG discrimination results comparing control versus player Correct Go (solid) and Correct No-Go (dashed) trials. (b) Sliding window discrimination of player versus controls by subject after transformation of the each subject's trials  $y$ -values. The solid and dashed horizontal lines indicate the  $p < 0.05$  FDR-corrected thresholds (c) A selection of significant Correct Go windows found from (b) showing brain regions that positively (red) and negatively (blue) correlate with subject expertise at specified time windows. (d) A selection of significant Correct No-Go windows found from (b) showing brain regions that positively (red) and negatively (blue) correlate with subject expertise at specified time windows. Statistical maps were thresholded at  $z > 1.8$ , and clusters were multiple-comparison corrected at  $p = 0.05$ . Tables 2 and 3 detail the cluster locations and sizes for activations shown in (c) and (d).**

(b). Correct Go trials (solid) had a maximum AUC of 0.89 at 350 ms, while Correct No-Go trials (dashed) had a maximum AUC of 0.95 at 325 ms. Significance thresholds are plotted as horizontal lines and are set at  $p < 0.05$  FDR-corrected for multiple windows.

The expertise rating  $y$ -values from the significant windows from the EEG analysis [Fig. 3(b)] were used as covariates of interest in finding areas of the brain that correlate with the EEG expertise measures derived across the trial duration. For Correct Go trials, significant clusters were found in almost all of the significant EEG expertise windows [Fig. 3(c)]. Negative correlations were found more in the earlier time windows ( $< 400$  ms). Significant positive correlation clusters were found in regions overlapping with the traditional player  $>$  control contrasts. Significant negative correlation clusters were found during the 125-ms window in the intracalcarine cortex and precuneus, during the 275-ms window in the superior lateral occipital cortex (LOC) and middle frontal gyrus, and during the 375-ms window in the inferior LOC. For positive correlations, significant clusters were found distributed across the entire cortex and trial duration. Significant positive correlation clusters were found during the 250-ms window in the precentral gyrus and SMA, during the 275-ms window in the superior frontal gyrus (SFG) and middle temporal gyrus (MTG), during the 375-ms window in the hippocampus and fusiform gyrus, during the 425-ms window in the posterior

cingulate, and during the 525-ms window in the supra marginal gyrus among others (Table 2).

For Correct No-Go trials, significant clusters were found in almost all of the significant time windows [Fig. 3(d)]. Negative correlations were found more in the later time windows ( $> 400$  ms) after the peak of expertise discrimination. Significant positive correlation clusters were found in regions overlapping with the traditional player  $>$  control contrasts. However, significant clusters in the correlation analysis are distributed far more broadly than in the traditional analysis. Positively correlated clusters were found during the 225-ms window in the SMA, temporal and frontal poles, during the 275-ms window in the SFG, lingual gyrus, and central opercular cortex, during the 375-ms window in the hippocampus and inferior LOC. Negatively correlated clusters were found during the 250-ms window in the middle frontal gyrus (MFG), during the 350-ms window in the occipital pole, during the 375-ms window in the subcallosal cortex, during the 400-ms window in the superior frontal gyrus, during the 425-ms window in the preSMA, and during the 475-ms window in the inferior LOC among others (Table 3).

### E. Structural Connectivity Differences Between Player Versus Control

To complement our functional connectivity analysis, we also analyzed the DTI data to identify structural networks

Table 2 Correct Go trial EEG-fMRI Fusion Results. Significant Clusters Found by the Simultaneous EEG-fMRI Methodology for Correct Go Trials [Fig. 3(c)]

Window (ms)	+/- Expertise Correlation	Max Z	# Voxels	Cluster $p$	Hemi	MNI-X (mm)	MNI-Y (mm)	MNI-Z (mm)	Brain Region
125	-	6.73	7106	2.04E-11	R	2	-78	50	Lateral Occipital Cortex
	-	5.27	2454	6.25E-05	L	-32	-66	-16	Cerebellum
	+	4.14	1097	0.0252	L	-54	-26	-14	Middle Temporal Gyrus
250	+	5.6	938	0.0028	R	2	-14	64	Precentral Gyrus
275	-	5.62	3466	3.58E-07	R	8	-78	50	Precuneus Cortex
	-	4.52	1105	0.0129	L	-38	-70	18	Lateral Occipital Cortex
	-	5.39	1039	0.0187	R	46	28	36	Middle Frontal Gyrus
	+	4.62	1491	0.00168	L	-12	20	68	Superior Frontal Gyrus
	+	4.19	883	0.0461	L	-50	-34	0	Middle Temporal Gyrus
300	-	7.14	2734	3.58E-06	L	-8	-80	48	Lateral Occipital Cortex
	-	4.23	895	0.0348	R	46	4	22	Precentral Gyrus
	+	4.64	2190	4.01E-05	L	-8	38	50	Superior Frontal Gyrus
	+	4.29	1212	0.00548	L	-58	-20	-4	Middle Temporal Gyrus
325	-	5.45	877	0.0112	R	10	-68	54	Precuneus Cortex
	+	3.55	969	0.00577	L	-66	-24	-10	Middle Temporal Gyrus
	+	4.03	855	0.0132	L	-12	48	46	Superior Frontal Gyrus
350	+	4.16	2122	2.12E-05	L	-62	-38	6	Middle Temporal Gyrus
	+	4.28	1585	0.000349	L	-20	28	56	Superior Frontal Gyrus
375	-	3.96	784	0.029	L	-28	-88	14	Lateral Occipital Cortex
	+	4.17	1255	0.00119	R	2	-78	-14	Cerebellum
400	+	5.14	702	0.0228	R	48	40	16	Frontal Pole
425	+	3.75	722	0.0217	R	2	-22	78	Precuneus Cortex
450	+	4.12	708	0.0201	R	40	48	2	Frontal Pole
475	+	4.68	1171	0.00104	L	-12	-76	-6	Cerebellum
	+	4.31	721	0.0293	L	-44	18	-6	Left Hippocampus

(continued on the next page)

Table 2 (continued)

Window (ms)	+/- Expertise Correlation	Max Z	# Voxels	Cluster $p$	Hemi	MNI-X (mm)	MNI-Y (mm)	MNI-Z (mm)	Brain Region
500	+	4.24	1256	0.00109	R	44	32	0	Frontal Pole
	+	3.29	994	0.00615	R	22	-64	-18	Cerebellum
	+	4.14	980	0.00677	R	46	-60	34	Postcentral Gyrus
	+	4.06	739	0.0382	L	-4	-72	0	Lingual Gyrus
525	+	5.2	6188	5.73E-10	R	8	-68	-6	Cerebellum
	+	3.79	2026	0.000493	R	52	-8	48	Precentral Gyrus
	+	5.18	1916	0.000775	R	46	6	30	Frontal Pole
	+	4.18	1193	0.0194	L	-56	-50	-12	Lateral Occipital Cortex
550	+	4.79	1589	0.000661	L	-6	-70	-2	Lingual Gyrus
	+	4.16	1432	0.00151	L	-18	-34	62	Postcentral Gyrus
	+	5.66	1128	0.00814	L	-62	-60	14	Lateral Occipital Cortex
	+	3.87	877	0.0364	R	46	18	12	Frontal Pole
575	+	4.21	1568	6.74E-05	L	-58	-56	0	Middle Temporal Gyrus
600	+	4.42	2127	8.40E-06	L	-52	-66	-20	Lateral Occipital Cortex
	+	4.52	832	0.0211		0	-78	-20	Cerebellum
625	+	6.14	1975	8.40E-05	L	-48	-66	-18	Lateral Occipital Cortex
	+	5.05	1177	0.00558	R	42	40	28	Middle Frontal Gyrus
	+	4.07	881	0.033	R	2	-16	-16	Right Thalamus
650	+	5.64	12106	2.93E-16	L	-22	-84	-26	Cerebellum
	+	5.66	3418	3.10E-06	R	6	-10	56	Precentral Gyrus

that differentiate the two groups [42]. Whole brain tractography analysis showed a robust structural network of nodes derived from the AAL atlas across all subjects [Fig. 4(a)]. The modular organization of the structural network found five communities of nodes across the brain [Fig. 4(b)]. Communities were roughly organized by hemisphere (LH-1,4;RH-2,3), cortical/subcortical motor and frontal regions (modules 1 and 2), visual/occipital regions (modules 3 and 4), and cerebellar regions (module 5). We first examined expertise-related structural effects by directly comparing the strength of structural connectivity between brain regions, and we found that players had 1.7 times as many

connections as the controls, 548 in players versus 328 in controls [ $p < 0.05$ , uncorrected, Fig. 4(c)]. Additionally, the difference in structural connectivity was mostly found between modules [Fig. 4(d)-left panel], including a significant difference between module 1 and module 5 ( $p < 0.0026$ ) for players versus controls [Fig. 4(d)-right panel].

#### IV. DISCUSSION

In this work, we used multimodal neuroimaging to identify structural and functional brain networks that differentiate a group of baseball players from a control group

**Table 3** Correct No-Go trial EEG-fMRI Fusion Results. Significant Clusters Found by the Simultaneous EEG-fMRI Methodology for CORRECT NoGo Trials [Fig. 3(d)]

Window (ms)	+/- Expertise Correlation	Max Z	# Voxels	Cluster $p$	Hemi	MNI-X (mm)	MNI-Y (mm)	MNI-Z (mm)	Brain Region
225									
	+	4.08	4878	1.89E-09	L	-52	4	-22	Temporal Pole
	+	4.93	4544	5.99E-09	R	54	-6	-22	Temporal Pole
	+	4.51	1930	0.000193	R	4	66	26	Frontal Pole
	+	4.42	948	0.0308	R	4	-12	60	Precentral Gyrus
250									
	-	4.84	915	0.0138	R	40	4	42	Middle Frontal Gyrus
	+	4.58	2276	5.30E-06	R	52	-2	-18	Temporal Pole
	+	3.93	1565	0.000243	L	-58	-16	-4	Temporal Pole
	+	3.68	947	0.0111	R	10	54	24	Frontal Pole
275									
	+	4.46	4247	5.96E-08	R	50	-32	26	Central Opercular Cortex
	+	4	2691	1.76E-05	L	-36	2	-16	Temporal Pole
	+	4.08	2331	7.45E-05	L	-12	-74	-12	Lingual Gyrus
	+	4.39	1671	0.00129	L	-2	54	0	Frontal Pole
	+	4.81	1501	0.00285	R	4	-76	34	Occipital Pole
	+	4.33	1287	0.00807	R	2	-48	70	Postcentral Gyrus
	+	4.29	1100	0.0209	L	-26	28	42	Superior Frontal Gyrus
300									
	+	4.19	4974	2.16E-10	R	54	-2	-18	Temporal Pole
	+	6.45	3371	1.19E-07	L	-56	-68	2	Middle Temporal Gyrus
	+	4.15	1713	0.000232	L	-14	22	64	Superior Frontal Gyrus
325									
	+	4.17	2149	8.34E-06	L	-48	-52	-4	Middle Temporal Gyrus
	+	3.95	1506	0.000293	L	-12	50	46	Superior Frontal Gyrus
	+	3.98	1269	0.00123	R	44	2	-22	Temporal Pole
350									
	-	5.79	861	0.017	L	-26	-90	-18	Occipital Pole
	+	5.79	3493	1.11E-08	L	-52	-74	-2	Left Hippocampus
	+	4.17	1192	0.00184	R	60	-8	-10	Temporal Pole
	+	4.56	770	0.0328	R	2	-92	18	Cuneal Cortex
375									
	-	3.75	691	0.0323	L	-2	28	-20	Subcallosal Cortex
	+	5.43	2237	1.01E-06	L	-46	-68	6	Lateral Occipital Cortex
	+	3.69	794	0.014	R	60	-8	-10	Temporal Pole

(continued on the next page)

Table 3 (continued)

400								
-	3.39	1969	3.34E-05	R	8	32	-18	Frontal Medial Cortex
-	3.64	1187	0.00276	R	30	52	16	Frontal Pole
-	4.59	887	0.0191	R	48	10	48	Middle Frontal Gyrus
-	5.41	818	0.0306	R	34	-82	-4	Occipital Pole
-	4.05	809	0.0325	R	44	-72	38	Lateral Occipital Cortex
-	5.21	803	0.0339	L	-36	-74	4	Occipital Pole
+	3.34	1168	0.00311	L	-36	-32	20	Superior Temporal Gyrus
425								
-	4.88	2479	5.78E-06	L	-4	-14	74	Precentral Gyrus
-	3.96	1646	0.000344	R	26	42	32	Frontal Pole
-	6.65	1481	0.000833	L	-38	-76	8	Cerebellum
-	4.32	1391	0.00137	R	24	-96	-8	Occipital Pole
450								
-	5.1	2430	1.97E-06	L	-16	-90	-18	Cerebellum
-	5.47	2230	5.42E-06	R	30	-94	-10	Lateral Occipital Cortex
-	3.8	1342	0.000777	R	8	28	-16	Subcallosal Cortex
-	4.72	937	0.0107		0	-4	60	Superior Frontal Gyrus
-	4.32	771	0.0343	R	18	60	-4	Frontal Pole
-	5.08	731	0.0459	R	40	8	36	Middle Frontal Gyrus
+	4.62	742	0.0424	L	-50	-72	12	Lateral Occipital Cortex
475								
-	5.09	2223	9.18E-06	L	-42	-14	54	Precentral Gyrus
-	5.69	2214	9.60E-06	L	-24	-86	-14	Cerebellum
-	5.95	2032	2.43E-05	R	40	-82	-2	Occipital Pole
-	3.46	852	0.0243	L	-2	22	-20	Subcallosal Cortex
-	4.12	830	0.0283	R	36	4	28	Middle Frontal Gyrus
+	5.16	2343	5.07E-06	L	-48	-64	-16	Lateral Occipital Cortex
+	4.11	1254	0.00184	L	-8	-76	-14	Lingual Gyrus
+	4.87	810	0.0324	L	-2	-78	20	Cuneal Cortex
500								
-	3.86	2226	2.62E-06	R	18	60	24	Frontal Pole
-	5.36	1546	0.000129	R	44	-58	-16	Occipital Pole
-	4.97	1067	0.00287	L	-46	-76	0	Occipital Pole
+	5.43	1143	0.00171	R	26	-76	26	Lingual Gyrus
+	4.01	695	0.0442	L	-56	-62	-2	Inferior Temporal Gyrus

when they performed a Go/No-Go task designed to mimic the situation of hitting a baseball. Below we discuss how our novel multimodal fusion approach advances our understanding of the structural and functional correlates of

expertise, specifically expertise in hitting a baseball, while also relating it to previous work on rapid decision making.

This study demonstrates that simultaneously acquired EEG-fMRI can be used to infer functional networks and

Table 3 (continued)

525								
-	4.24	3397	1.05E-08	L	-2	60	4	Frontal Pole
-	4.99	1652	8.47E-05	R	44	-60	-18	Occipital Pole
-	4.99	1455	0.000277	L	-28	-94	-16	Occipital Pole
-	3.75	739	0.0354	L	-34	-62	-22	Cerebellum
550								
-	3.82	3165	5.96E-08	R	20	64	4	Frontal Pole
-	5.49	2482	2.09E-06	R	40	-80	0	Occipital Pole
-	4.43	1671	0.000143	L	-36	-72	8	Occipital Pole
-	4	753	0.0445	L	-32	-52	-36	Cerebellum
+	3.95	867	0.02	L	-50	-62	-12	Middle Temporal Gyrus
575								
+	3.34	929	0.00398	L	-42	-36	-16	Middle Temporal Gyrus
600								
-	4	705	0.0245	R	20	-100	-2	Occipital Pole
+	3.62	955	0.00326	L	-46	-22	12	Middle Temporal Gyrus
675								
-	3.43	815	0.039		0	42	2	Frontal Pole
+	5.37	4079	4.65E-09	R	22	-70	46	Precentral Gyrus
+	5.91	2102	2.69E-05	R	50	-62	-20	Cerebellum
+	5.68	810	0.0403	L	-60	-64	2	Lateral Occipital Cortex
725								
-	3.96	1535	0.000127		0	62	6	Frontal Pole

offer confirmatory evidence for source localization findings, including those estimated from EEG-only acquisitions [20]. Since source localization is an ill-posed problem, the localization cannot be considered conclusive; however, simultaneous EEG-fMRI enables a within-subject and within-trial comparison of the brain regions identified in functional analyses from the complementary neuroimaging methodologies. Here, we show that activity in fusiform gyrus that was identified in our traditional fMRI analysis of group differences between players and controls [Fig. 2(b) and (c)] matched our EEG findings that players have a larger activation in a source localized in the fusiform region. This confirmatory, multimodal result adds to the growing literature that the fusiform gyrus plays a significant role in the expertise-dependent visual object recognition [43]–[47]. Players also had a larger activation in the middle temporal gyrus (MTG) specifically in the left visual area MT/V5 complex which may also give players superior performance as this area is implicated in motion processing. Another area where players exhibited stronger activations was the supra-marginal gyrus. This

area is part of the action observation network (AON) and plays a role in the somatosensory processing stream. Surprisingly, we also see activation in the SMA in both the Correct Go and Correct No-Go player/control contrasts. The location of this activation is similar to the area found in our previous Correct No-Go EEG source localization results [20], providing confirmatory evidence that players preferentially activate their SMA, relative to controls, during this baseball-like task. SMA regions, including the pre-SMA, have a known role in motor learning [48]–[51] and critical involvement during Go/No-Go tasks which probe inhibitory control circuits [20], [52]–[56].

In addition to confirming previous results, simultaneously acquired EEG-fMRI allows for a more comprehensive understanding of the differences between players and controls with respect to the spatiotemporal cascade of activity across the brain. Our novel methodology identifies multiple poststimulus 50-ms windows with predictive EEG neural correlates of expertise and fuses these temporal windows with fMRI activity in a whole-brain 2-mm voxel analysis, revealing time-localized correlations

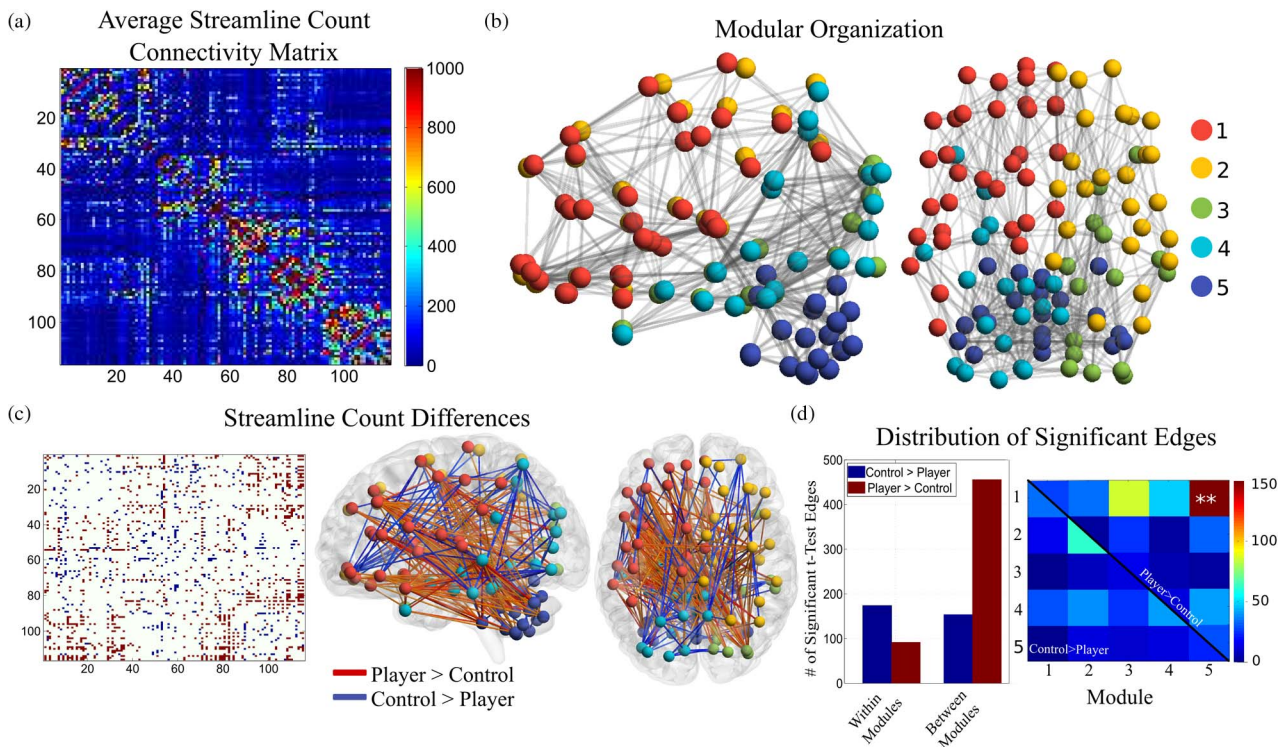


**Fig. 4. Structural network organization and differences related to expertise. (a) Average structural connectivity matrix reorganized by its modular organization. Edges are streamline counts that pass between AAL atlas regions of interest. (b) Three-dimensional sagittal and axial views of the structural networks in anatomical space displaying the top 0.5% of connections. (c) Structural connectivity matrix group differences ( $p < 0.05$ , uncorrected) displaying expert baseball players > controls (red) and controls > players (blue) for streamline counts in the connectivity matrix and 3-D brain space. (d) Number of player > control (red) and control > player between group connections differing for within-module and between-module connections (left) and specific module-to-module results (right). Significance ( $p < 0.05$  FDR corrected) for module-to-module differences was computed by 5000 permutations. Significant module-to-module differences are marked by “\*\*.”**

of expertise at a spatial scale of millimeters. Many of the significant regions found in the fusion analysis were also observed in the traditional player versus controls contrast, though the fusion analysis enabled a deconstruction of this activity across time. Additionally, some areas that significantly correlate with expertise in the fused analysis were not present in the traditional analysis, including the SFG, the hippocampus, and all regions with significant negative correlations [Fig. 3(c) and (d)]. These novel spatiotemporal findings suggest that the fused approach may provide more sensitivity than a traditional fMRI-only GLM analysis. Interestingly, the fused approach identified regions in early visual processing areas—the temporal occipital fusiform cortex (TOFC), parahippocampal gyrus, and paracingulate gyrus. Activity in these regions were significantly correlated with expertise, and they are the same areas known to be used in Bar’s visual prediction theory [57]. In addition, significant positive correlations in the right SFG at 275 and 300 ms for Correct Go and Correct No-Go trials maps directly to a region known to integrate information from the visual processing areas [58]. This functional evidence taken together helps to support the

theory that expertise—specifically, sportive expertise—can produce more efficient neural processing for domain specific perceptual tasks [59]–[61].

This novel fusion methodology is fully data-driven and uses the entire EEG sensor and fMRI voxel space to identify the functional cascade that differentiates two groups. To date, the majority of EEG-fMRI studies use correlative measures to inspect the EEG-informed BOLD modulations [62], and relatively little previous work has used EEG-fMRI fusion methodologies to identify differences between subject populations. One recent exception is [63], who used a joint independent component analysis (jICA, [64]) with simultaneous EEG-fMRI to show that schizophrenic patients have marked differences in processing oddball stimuli compared to controls, but their methodology only used a single electrode for the EEG analysis and requires user supervision to determine ICA components.

Our data-driven methodology takes a more complementary approach to fuse neural information across EEG and fMRI methodologies since it is well known that each neuroimaging measurement may reflect characteristics of

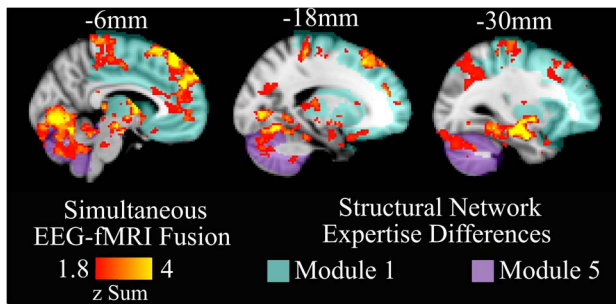


**Fig. 5. Functional and structural group difference overlap.** Functional EEG-fMRI fusion results for Correct Go trials summed across significant temporal windows displayed on the MNI brain. Structural modular regions that were found to have significantly more player > novice streamlines between them (module 1—green and module 5—purple) are also displayed. Functional fusion activations of player > control overlap with the structural regions that show differences between groups.

different populations of cells [65]. Here, we use all EEG electrodes to identify temporal windows with neural correlates of expertise that can successfully classify players versus controls and then use this temporal information in a whole-brain GLM analysis of fMRI data to investigate which regions of the brain covary with the predictive EEG signals of expertise. While our results confirm the promise of our EEG-fMRI fusion approach, future research should continue to explore additional methods to extract the strengths of each neuroimaging modality and mitigate known weaknesses, allowing additional hybrid analyses to expand our understanding of relationships between complementary neuroimaging signals.

Our fusion approach for simultaneously collected EEG and fMRI data provides a functional mapping of expertise related differences between the players and controls. It is also important to identify and understand if there are structural differences between the groups. Structural connectivity analysis showed that the players have significantly more coherent structural connections between cerebellar and left frontal/motor regions [Fig. 4(d)]. These trends point to the players having neuroplastic changes specific to motor processing regions of the brain. This is more clearly shown in the overlap between the functional activations from the EEG-fMRI fusion and the structural connectivity (Fig. 5). This fronto-cerebellar pattern is particularly interesting given that there is a well-established pattern of connectivity between lateral frontal areas and lateral regions of the cerebellum, consistent with the location of expertise predicting activity in our task [66]. Rather than regulating motor coordination,

as is usually assumed with cerebellar pathways, these cortical-cerebellar networks are thought to regulate the integration of high-level executive and attention processes that are critical for efficient, adaptive decision making [67]. We found that expert players have greater network-level communication, at both the structural and functional levels, between these fronto-cerebellar circuits. This between-module communication is a plausible neural substrate that can explain the improved behavioral performance at a sensory discrimination task with minimal movement control demands.

In summary, our results indicate a difference in the unfolding of cognitive processes for players versus controls and that these functional differences may at least be partially a result of differences in structural networks between the groups. We find correlative evidence that these macroscale neural differences translate into higher behavioral accuracies and faster response times in players. The spatiotemporal cascade reflecting these differences between the groups begins as early as 200 ms after the pitch starts and lasting up to 700 ms afterwards. Network differences are spatially localized to include motor and visual processing areas, providing evidence for differences in perception-action coupling between the groups. These findings reinforce many studies implicating these areas in mediating visual prediction and expertise [43], [47], [57], [68]–[70]. We also find that our results confirm many prior fMRI studies showing that athletes have stronger activations in the action observation network while they observed or listened to the domain of their expertise [59]–[61], [71]–[76].

In general, our approach illustrates how multimodal neuroimaging can provide specific macroscale insights into the functional and structural correlates of expertise development. This approach, however, may also capture underlying physiology that can account for variability in performance, whether it arises from between subject differences due to genetic or experimental factors or from within subject variability due to fluctuations in attention, interest, etc. Future work should examine the sensitivity of this multimodal approach to capture variability across varying levels of expertise, providing a framework to reveal how brain connectivity enables superior performance. ■

## Acknowledgment

J. Mursakin and J. Sherwin are cofounders of deCervo, a private company that provides neuroprofiles for athletes. T. Verstynen has equity interest in Neuroscouting, a private company that provides services to baseball players.

## REFERENCES

- [1] R. Yuste, "From the neuron doctrine to neural networks," *Nature Rev. Neurosci.*, vol. 16, no. 8, pp. 487–497, 2015.
- [2] A. Bertrand et al., "Beamforming approaches for untethered, ultrasonic neural dust motes for cortical recording: A simulation study," *Proc. Annu. Int. Conf. IEEE Eng. Med. Biol. Soc.*, vol. 2014, pp. 2625–2628, 2014.
- [3] D. Seo, J. M. Carmena, J. M. Rabaey, M. M. Maharbiz, and E. Alon, "Model validation of untethered, ultrasonic neural dust motes for cortical recording."

- J. Neurosci. Methods*, vol. 244, pp. 114–122, 2015.
- [4] E. Fouragnan, C. Retzler, K. Mullinger, and M. G. Philiastides, “Two spatiotemporally distinct value systems shape reward-based learning in the human brain,” *Nature Commun.*, vol. 6, p. 8107, 2015.
  - [5] S. Dahne et al., “Multivariate machine learning methods for fusing multimodal functional neuroimaging data,” *Proc. IEEE*, vol. 103, no. 9, pp. 1507–1530, 2015.
  - [6] R. I. Goldman and J. M. Stern, “Simultaneous EEG and fMRI of the alpha rhythm,” *Neuroreport*, vol. 13, no. 18, pp. 2487, 2002.
  - [7] R. I. Goldman et al., “Single-trial discrimination for integrating simultaneous EEG and fMRI: Identifying cortical areas contributing to trial-to-trial variability in the auditory oddball task,” *NeuroImage*, vol. 47, pp. 136–147, 2009.
  - [8] J. Jorge, W. van der Zwaag, and P. Figueiredo, “EEG-fMRI integration for the study of human brain function,” *NeuroImage*, vol. 102, pp. 24–34, 2014.
  - [9] J. M. Walz et al., “Simultaneous EEG-fMRI reveals temporal evolution of coupling between supramodal cortical attention networks and the brainstem,” *J. Neurosci.*, vol. 33, no. 49, pp. 19212–19222, 2013.
  - [10] J. M. Walz et al., “Simultaneous EEG-fMRI reveals a temporal cascade of task-related and default-mode activations during a simple target detection task,” *NeuroImage*, vol. 102 Pt 1, pp. 229–239, 2014.
  - [11] J. M. Walz et al., “Premodulus EEG alpha oscillations modulate task-related fMRI BOLD responses to auditory stimuli,” *NeuroImage*, vol. 113, pp. 153–163, 2015.
  - [12] D. Le Bihan and H. Johansen-Berg, “Diffusion MRI at 25: Exploring brain tissue structure and function,” *NeuroImage*, vol. 61, no. 2, pp. 324–341, 2012.
  - [13] C. Sampaio-Baptista et al., “Motor skill learning induces changes in white matter microstructure and myelination,” *J. Neurosci.*, vol. 33, no. 50, pp. 19499–19503, 2013.
  - [14] P. Hagmann et al., “Understanding diffusion MR imaging techniques: From scalar diffusion-weighted imaging to diffusion tensor imaging and beyond,” *Radiographics*, vol. 26, pp. S205–S223, 2006.
  - [15] S. L. Bengtsson et al., “Extensive piano practicing has regionally specific effects on white matter development,” *Nature Neurosci.*, vol. 8, no. 9, pp. 1148–1150, 2005.
  - [16] J. Scholz, M. C. Klein, T. E. Behrens, and H. Johansen-Berg, “Training induces changes in white-matter architecture,” *Nature Neurosci.*, vol. 12, no. 11, pp. 1370–1371, 2009.
  - [17] R. L. Muetzel et al., “The development of corpus callosum microstructure and associations with bimanual task performance in healthy adolescents,” *NeuroImage*, vol. 39, no. 4, pp. 1918–1925, 2008.
  - [18] A. N. Voineskos et al., “Age-related decline in white matter tract integrity and cognitive performance: A DTI tractography and structural equation modeling study,” *Neurobiol. Aging*, vol. 33, no. 1, pp. 21–34, 2012.
  - [19] P. Recer, “Hitting fastball ‘clearly impossible,’” *Cape Breton Post*, 2000, pp. 11/FRONT.
  - [20] J. Muraskin, J. Sherwin, and P. Sajda, “Knowing when not to swing: EEG evidence that enhanced perception-action coupling underlies baseball batter expertise,” *NeuroImage*, vol. 123, pp. 1–10, 2015.
  - [21] J. S. Sherwin, J. Muraskin, and P. Sajda, “Pre-stimulus functional networks modulate task performance in time-pressured evidence gathering and decision-making,” *NeuroImage*, vol. 111, pp. 513–525, 2015.
  - [22] A. M. Dale, “Optimal experimental design for event-related fMRI,” *Human Brain Mapping*, vol. 8, no. 2/3, pp. 109–114, 1999.
  - [23] J. Sherwin, J. Muraskin, and P. Sajda, “You can’t think and hit at the same time: Neural correlates of baseball pitch classification,” *Front. Neurosci.*, vol. 6, p. 177, 2012.
  - [24] D. H. Brainard, “The psychophysics toolbox,” *Spatial Vis.*, vol. 10, pp. 433–436, 1997.
  - [25] P. Sajda, R. I. Goldman, M. G. Philiastides, A. D. Gerson, and T. R. Brown, “A system for single-trial analysis of simultaneously acquired EEG and fMRI,” *Proc. 3rd Int. IEEE/EMBS Conf. Neural Eng.*, 2007.
  - [26] A. Delorme and S. Makeig, “EEGLAB: An open source toolbox for analysis of single-trial EEG dynamics including independent component analysis,” *J. Neurosci. Methods*, vol. 134, no. 1, pp. 9–21, 2004.
  - [27] A. Hyvarinen, “Fast and robust fixed-point algorithms for independent component analysis,” *IEEE Trans. Neural Netw.*, vol. 10, no. 3, pp. 626–634, 1999.
  - [28] L. C. Parra, C. D. Spence, A. D. Gerson, and P. Sajda, “Recipes for the linear analysis of EEG,” *NeuroImage*, vol. 28, no. 2, pp. 326–341, 2005.
  - [29] J. Sherwin and P. Sajda, “Musical experts recruit action-related neural structures in harmonic anomaly detection: Evidence for embodied cognition in expertise,” *Brain Cogn.*, vol. 83, no. 2, pp. 190–202, 2013.
  - [30] M. I. I. Jordan and R. A. A. Jacobs, “Hierarchical mixtures of experts and the EM algorithm,” *Neural Comput.*, vol. 6, no. 2, pp. 181–214, 1994.
  - [31] S. M. Smith et al., “Advances in functional and structural MR image analysis and implementation as FSL,” *NeuroImage*, vol. 23 Suppl 1, pp. S208–219, 2004.
  - [32] R. E. Kelly et al., “Visual inspection of independent components: Defining a procedure for artifact removal from fMRI data,” *J. Neurosci. Methods*, vol. 189, no. 2, pp. 233–245, 2010.
  - [33] G. Strang, “Introduction to linear algebra,” *Math. Comput.*, vol. 18, p. 510, 2003.
  - [34] K. J. Worsley, “Detecting activation in fMRI data,” *Stat. Methods Med. Res.*, vol. 12, pp. 401–418, 2003.
  - [35] M. G. Philiastides and P. Sajda, “EEG-informed fMRI reveals spatiotemporal characteristics of perceptual decision making,” *J. Neurosci.*, vol. 27, no. 48, pp. 13082–13091, 2007.
  - [36] F. C. Yeh, P. F. Tang, and W. Y. Tseng, “Diffusion MRI connectometry automatically reveals affected fiber pathways in individuals with chronic stroke,” *NeuroImage Clin.*, vol. 2, pp. 912–921, 2013.
  - [37] F. C. Yeh, V. J. Wedeen, and W. Y. Tseng, “Estimation of fiber orientation and spin density distribution by diffusion deconvolution,” *NeuroImage*, vol. 55, no. 3, pp. 1054–1062, 2011.
  - [38] F. C. Yeh, T. D. Verstynen, Y. Wang, J. C. Fernandez-Miranda, and W. Y. Tseng, “Deterministic diffusion fiber tracking improved by quantitative anisotropy,” *PLoS One*, vol. 8, no. 11, 2013, Art. no. e80713.
  - [39] A. Griffa, P. S. Baumann, J. P. Thiran, and P. Hagmann, “Structural connectomics in brain diseases,” *NeuroImage*, vol. 80, pp. 515–526, 2013.
  - [40] M. Rubinov and O. Sporns, “Complex network measures of brain connectivity: Uses and interpretations,” *NeuroImage*, vol. 52, no. 3, pp. 1059–1069, 2010.
  - [41] J. D. Rudie et al., “Altered functional and structural brain network organization in autism,” *NeuroImage Clin.*, vol. 2, pp. 79–94, 2012.
  - [42] T. Verstynen, K. Jarbo, S. Pathak, and W. Schneider, “In vivo mapping of microstructural somatotopies in the human corticospinal pathways,” *J. Neurophysiol.*, vol. 105, no. 1, pp. 336–346, 2011.
  - [43] I. Gauthier, M. J. Tarr, W. Anderson, P. Skudlarski, and J. C. Gore, “Activation of the middle fusiform ‘face area’ increases with expertise in recognizing novel objects,” *Nature Neurosci.*, vol. 2, no. 6, pp. 568–573, 1999.
  - [44] R. W. McGugin, J. C. Gatenby, J. C. Gore, and I. Gauthier, “High-resolution imaging of expertise reveals reliable object selectivity in the fusiform face area related to perceptual performance,” *Proc. Nat. Acad. Sci. USA*, vol. 109, no. 42, pp. 17063–17068, 2012.
  - [45] Y. Xu, “Revisiting the role of the fusiform face area in visual expertise,” *Cereb. Cortex*, vol. 15, pp. 1234–1242, 2005.
  - [46] M. Bilalić, L. Turella, G. Campitelli, M. Erb, and W. Grodd, “Expertise modulates the neural basis of context dependent recognition of objects and their relations,” *Human Brain Mapping*, vol. 33, pp. 2728–2740, 2012.
  - [47] M. Bilalić, R. Langner, R. Ulrich, and W. Grodd, “Many faces of expertise: Fusiform face area in chess experts and novices,” *J. Neurosci.*, vol. 31, no. 28, pp. 10206–10214, 2011.
  - [48] K. Sakai et al., “Activation of human presupplementary motor area in learning of sequential procedures: A functional MRI study,” *J. Neurophysiol.*, vol. 76, no. 1, pp. 617–621, 1996.
  - [49] H. Aizawa, M. Inase, H. Mushiake, K. Shima, and J. Tanji, “Reorganization of activity in the supplementary motor area associated with motor learning and functional recovery,” *Exp. Brain Res.*, vol. 76, pp. 668–671, 1991.
  - [50] U. Halsband and H. J. Freund, “Premotor cortex and conditional motor learning in man,” *Brain*, vol. 113, no. 1, pp. 207–222, 1990.
  - [51] U. Halsband and R. K. Lange, “Motor learning in man: A review of functional and clinical studies,” *J. Physiol.*, vol. 99, no. 4–6, pp. 414–424, 2006.
  - [52] D. J. Simmonds, J. J. Pekar, and S. H. Mostofsky, “Meta-analysis of Go/No-go tasks demonstrating that fMRI activation associated with response inhibition is task-dependent,” *Neuropsychologia*, vol. 46, no. 1, pp. 224–232, 2008.
  - [53] M. J. Frank et al., “fMRI and EEG predictors of dynamic decision parameters during human reinforcement learning,” *J. Neurosci.*, vol. 35, no. 2, pp. 485–494, 2015.
  - [54] B. U. Forstmann et al., “Cortico-striatal connections predict control over speed and accuracy in perceptual decision making,”

- Proc. Nat. Acad. Sci. USA*, vol. 107, no. 36, pp. 15 916–15 920, 2010.
- [55] K. Dunovan, B. Lynch, T. Molesworth, and T. Verstynen, “Competing basal ganglia pathways determine the difference between stopping and deciding not to go,” *Elife*, vol. 4, 2015.
- [56] S. Jahfari et al., “How preparation changes the need for top-down control of the basal ganglia when inhibiting premature actions,” *J. Neurosci.*, vol. 32, no. 32, pp. 10870–10878, 2012.
- [57] O. S. Cheung and M. Bar, “Visual prediction and perceptual expertise,” *Int. J. Psychophysiol.*, vol. 83, pp.156–163, 2012.
- [58] H. R. Heekeren, S. Marrett, P. Bandettini, and L. G. Ungerleider, “A general mechanism for perceptual decision-making in the human brain,” *Nature*, vol. 431, pp. 859–862, 2004.
- [59] G. Bernardi et al., “How skill expertise shapes the brain functional architecture: An fMRI study of visuo-spatial and motor processing in professional racing-car and naive drivers,” *PLoS One*, vol. 8, no. 10, pp. 1–11, 2013.
- [60] D. T. Bishop, M. J. Wright, R. C. Jackson, and B. Abernethy, “Neural bases for anticipation skill in soccer: An FMRI study,” *J. Sport Exercise Psychol.*, vol. 35, no. 1, pp. 98–109, 2013.
- [61] N. Balsler et al., “Prediction of human actions: Expertise and task-related effects on neural activation of the action observation network,” *Human Brain Mapping*, vol. 35, no. 8, pp. 4016–4034, 2014.
- [62] R. J. Huster, S. Debener, T. Eichele, and C. S. Herrmann, “Methods for simultaneous EEG-fMRI: An introductory review,” *J. Neurosci.*, vol. 32, no. 18, pp. 6053–6060, May 2012.
- [63] V. Calhoun, L. Wu, K. Kiehl, T. Eichele, and G. Pearlson, “Aberrant processing of deviant stimuli in schizophrenia revealed by fusion of FMRI and EEG data,” *Acta Neuropsychiatry*, vol. 22, no. 3, pp. 127–138, 2010.
- [64] T. Eichele et al., “Unmixing concurrent EEG-fMRI with parallel independent component analysis,” *Int. J. Psychophysiol.*, vol. 67, no. 3, pp. 222–234, 2008.
- [65] P. L. Nunez and R. Srinivasan, “*Electric Fields of the Brain: The Neurophysics of EEG*,” Oxford, U.K.Oxford Univ. Press, 2006.
- [66] P. L. Strick, R. P. Dum, and J. A. Fiez, “Cerebellum and nonmotor function,” *Annu. Rev. Neurosci.*, vol. 32, pp. 413–434, 2009.
- [67] N. Ramnani, “The primate cortico-cerebellar system: Anatomy and function,” *Nature Rev. Neurosci.*, vol. 7, no. 7, pp. 511–522, 2006.
- [68] M. Bar, “Predictions: A universal principle in the operation of the human brain. Introduction,” *Philosoph. Trans. Roy. Soc. Lond. B, Biol. Sci.*, vol. 364, pp. 1181–1182, 2009.
- [69] M. Bar, “The proactive brain: Memory for predictions,” *Philosoph. Trans. Roy. Soc. Lond. B, Biol. Sci.*, vol. 364, pp. 1235–1243, 2009.
- [70] K. Kveraga et al., “Early onset of neural synchronization in the contextual associations network,” *Proc. Nat. Acad. Sci. USA*, vol. 108, pp. 3389–3394, 2011.
- [71] J. Kim et al., “Neural correlates of pre-performance routines in expert and novice archers,” *Neurosci. Lett.*, vol. 445, no. 3, pp. 236–241, 2008.
- [72] Y. T. Kim et al., “Neural correlates related to action observation in expert archers,” *Behav. Brain Res.*, 2011, vol. 223, no. 2, pp. 342–347.
- [73] E. Woods, A. E. Hernandez, V. E. Wagner, and S. L. Beilock, “Expert athletes activate somatosensory and motor planning regions of the brain when passively listening to familiar sports sounds,” *Brain Cogn.*, vol. 87, pp. 122–133, 2014.
- [74] G. Rizzolatti and L. Craighero, “The mirror-neuron system,” *Annu. Rev. Neurosci.*, vol. 27, pp. 169–192, 2004.
- [75] B. Calvo-Merino, J. Grezes, D. E. Glaser, R. E. Passingham, and P. Haggard, “Seeing or doing? Influence of visual and motor familiarity in action observation,” *Curr. Biol.*, vol. 16, no. 19, pp. 1905–1910, 2006.
- [76] J. Milton, A. Solodkin, P. Hlustik, and S. L. Small, “The mind of expert motor performance is cool and focused,” *NeuroImage*, vol. 35, no. 2, pp. 804–813, 2007.

#### ABOUT THE AUTHORS

**Jordan Muraskin** received the B.S. degree in biomedical engineering and the Ph.D. degree from Columbia University, Columbia, NY, USA, in 2007 and 2015, respectively.

In 2007, he joined the Taub Institute for Research on Alzheimer’s Disease and the Aging Brain. His Ph.D work in the Laboratory for Intelligent Imaging and Neural Computing focused on fusing multimodal neuroimaging methodologies to study perceptual expertise. He is currently starting his ostdoctoral training in the Computational Neuroimaging Laboratory, Child Mind Institute.



**Jason Sherwin** received the B.A. degree in physics from the University of Chicago, Chicago, IL, USA, in 2005 and the M.S. and Ph.D. degrees in aerospace engineering from Georgia Institute of Technology, Atlanta, GA, USA, in 2006 and 2010, respectively.

He did his postdoctoral training at Columbia University, New York, NY, USA and was also a Research Assistant Professor in the Department of Ophthalmology, State University of New York Downstate Medical Center. Currently he is the cofounder and Chief Executive Officer of deCervo, a startup based in New York City that focuses on brain imaging of high-speed decision making.



**Gregory Lieberman** received the B.A. degree in psychology from the University of Massachusetts, Amherst, MA, USA, in 2003 and the Ph.D. degree in neuroscience from the University of Vermont, Burlington, VT, USA, in 2014.

He conducted predoctoral research at the MassGeneral Institute for Neurodegenerative Disease, Harvard Medical School; doctoral research at the MindBody Medicine Clinic and Clinical Neuroscience Research Unit, Fletcher Allen Healthcare; and an IARPA-funded postdoctoral fellowship in cognitive



neuroscience at the Psychology Clinical Neuroscience Center, University of New Mexico. He is currently a Postdoctoral Fellow at the Human Research and Engineering Directorate, U.S. Army Research Laboratory; a visiting scholar at the Department of Bioengineering, University of Pennsylvania; and a neuroscientific consultant for MINDSET, the consulting group of the Mind Research Network. His primary research interests include computational analyses of learning-related neuroplasticity, brain structure/function coupling relationships, and neurostimulation.

**Javier O. Garcia** received the B.A. degree in cognitive science from Rice University, Houston, TX, USA, in 2004 and the M.A. and Ph.D. degrees in cognitive neuroscience from the University of California, Irvine, Irvine, CA, USA, in 2009, with funding from the National Research Service Award from NIH-NEI.

In 2009, he began his postdoctoral work in the Human Neurodynamics Lab, University of California, Irvine and then he joined the Perception and Cognition Lab, University of California, San Diego, La Jolla, CA, USA, in 2011. His relationship with the U.S. Army Research Laboratory began in 2014 as a Joint Postdoctoral Researcher with Syntrogi Inc. (San Diego, CA, USA), and then he joined the lab a year later as a civilian Neuroscientist in the Human Research and Engineering Directorate under the Future Soldier Technology division. Using a variety of human neuroscientific techniques, his expertise and research interests include computational neuroimaging explorations linking neural measures to human behavior in several cognitive domains.



## Mursakin *et al.*: Fusing Multiple Neuroimaging Modalities to Assess Group Differences in Perception-Action Coupling

**Timothy Verstynen** received the B.A. degree in psychology from the University of New Mexico, Albuquerque, NM, USA, in 2001 and the Ph.D. degree in psychology from the University of California, Berkeley, Berkeley, CA, USA, in 2006.

He did postdoctoral training in neuroscience at the University of California, San Francisco, San Francisco, CA, USA, and cognitive neuroscience at the University of Pittsburgh, Pittsburgh, PA, USA, in 2009 and 2012, respectively. In 2012, he joined the Department of Psychology and Center for Neural Basis of Cognition, Carnegie Mellon University, Pittsburgh, PA, USA, as an Assistant Professor. He currently heads the Cognitive Axon Laboratory, where his research primarily focuses on understanding how the structure of sensorimotor pathways in the brain constrains learning and decision making.

Dr. Verstynen has received several awards for his research, including a National Science Foundation (NSF) CAREER award.



**Jean M. Vettel** received the Ph.D. degree in cognitive neuroscience from Brown University, Providence, RI, USA, funded by an NSF Graduate Fellowship (2004-2007) and a DoD SMART Fellowship (2007-2009), following a lab position at Washington University in St. Louis, St. Louis, MO, USA, and the B.A. degree from Carnegie Mellon University, Pittsburgh, PA, USA.

Since September 2009, she has been a civilian neuroscientist at the U.S. Army Research Laboratory (ARL) and leads the Brain Structure-Function Couplings research area in the Army's Translational Neuroscience mission program in the Future Soldier Technologies Division of the Human Research and Engi-



neering Directorate. In support of ARL's Open Campus research initiative, she was appointed as adjunct faculty at the University of California, Santa Barbara, Santa Barbara, CA, USA, in 2014 and a visiting scholar at the University of Pennsylvania, Philadelphia, PA, USA, in 2015. Her collaborative research investigates methods to quantify brain connectivity that accounts for task performance variability both within and between individuals and then uses these brain metrics in novel neurotechnology approaches to enhance the way that human and technology interact.

**Paul Sajda** (Fellow, IEEE) received the B.S. degree in electrical engineering from the Massachusetts Institute of Technology, Cambridge, MA, USA, in 1989 and the M.S. and Ph.D. degrees in bioengineering from the University of Pennsylvania, Philadelphia, PA, USA, in 1992 and 1994, respectively.

In 1994, he joined the David Sarnoff Research Center where he went on to become the Head of the Adaptive Image and Signal Processing Group. He is currently Professor of Biomedical Engineering, Electrical Engineering and Radiology at Columbia University, New York, NY, USA, where he is Director of the Laboratory for Intelligent Imaging and Neural Computing (LIINC). His research focuses on neural engineering, neuroimaging, computational neural modeling, and machine learning applied to image understanding.

Prof. Sajda has received several awards for his research including a National Science Foundation (NSF) CAREER Award and the Sarnoff Technical Achievement Award. He is an elected Fellow of the American Institute of Medical and Biological Engineering (AIMBE). He serves as the Editor-in-Chief of the IEEE TRANSACTIONS ON NEURAL SYSTEMS AND REHABILITATION and is the Chair of the IEEE Brain Initiative.

